Marine Pollution Bulletin 58 (2009) 1367–1373

Contents lists available at ScienceDirect

Marine Pollution Bulletin

journal homepage: www.elsevier.com/locate/marpolbul

The effects of wind and rainfall on suspended sediment concentration related to the 2004 Indian Ocean tsunami

XinFeng Zhang [a,b], DanLing Tang [b,*], ZiZhen Li [a,*], FengPan Zhang [c]

[a] Institute of Bioinformatics, School of Mathematics and Statistics, Lanzhou University, Lanzhou 730000, China
[b] Center of Remote Sensing on Marine Ecology/Environment (RSMEE), LED, South China Sea Institute of Oceanology, Chinese Academy of Sciences, Guangzhou 510301, China
[c] School of Mathematics and Information Sciences, Henan University, Kaifeng 475001, China

ARTICLE INFO

Keywords:
Indian Ocean tsunami
Suspended sediment concentrations
Sediment-associated contaminants
Wind
Rainfall
Spatial autocorrelation

ABSTRACT

The effects of rainfall and wind speed on the dynamics of suspended sediment concentration (SSC), during the 2004 Indian Ocean tsunami, were analyzed using spatial statistical models. The results showed a positive effect of wind speed on SSC, and inconsistent effects (positive and negative) of rainfall on SSC. The effects of wind speed and rainfall on SSC weakened immediately around the tsunami, indicating tsunami-caused floods and earthquake-induced shaking may have suddenly disturbed the ocean–atmosphere interaction processes, and thus weakened the effects of wind speed and rainfall on SSC. Wind speed and rainfall increased markedly, and reached their maximum values immediately after the tsunami week. Rainfall at this particular week exceeded twice the average for the same period over the previous 4 years. The tsunami-affected air–sea interactions may have increased both wind speed and rainfall immediately after the tsunami week, which directly lead to the variations in SSC.

1. Introduction

The Indian Ocean tsunami on 26 December 2004 was an unprecedented natural disaster. The marine and terrestrial environments along the coastal zones were massively damaged, which include extensive coastal erosion, contaminant dispersion and deposition, ground and surface water pollution, long-term impacts to coastal zone ecosystems, and widespread introduction of contaminated materials to the sea (Liu et al., 2005; UNEP, 2005; Dahdouh-Guebas and Koedam, 2006; Tang et al., 2009). The transport of sediment-associated contaminants (SAC), from the coastal land to the ocean, is especially important to the marine environment, because the subsequent dispersal directly affects biological productivity of the oceans (Eisma, 1981; Nittrouer and Kuehl, 1995; Witt and Siegel, 2000; Yan and Tang, 2008). In recent years, suspended sediment concentration (SSC) has been being used as a less costly and more easily measured surrogate for SAC in some coastal wasters (Leatherbarrow et al., 2005; Schoellhamer et al., 2003). Physical processes that affect SSC also largely affect SAC (Schoellhamer et al., 2007).

There are many oceanic and atmospheric factors (such as offshore distance, wind, rainfall, etc.) that influence SSC dynamics in the ocean (De Haas and Eisma, 1993; Ridderinkhof et al., 2000; Zheng and Tang, 2007). Also, various natural physical processes (such as tides, storm surge and waves) can significantly affect the spatial variability of SSC and associated SAC (Powell et al., 1989; Schoellhamer, 2002; Ramaswamy et al., 2004). Earthquakes and floods are the catastrophic events that typically bring about major changes to SSC and SAC in the coastal zones (Zonta et al., 2005). These large and abrupt events can also induce sudden changes in the ocean–atmosphere interactions, including anomalous behavior of numerous oceanic and atmospheric processes (Hayakawa et al., 1994; Krishnakutty, 2005). The spatial dynamics of SSC at the sea surface is one of these interaction processes.

The massive flooding caused by the 2004 Sumatra tsunami was unprecedented. This paper seeks to answer the question of whether, and to what extent, this tsunami-caused flood, together with other changes in marine environmental factors, affected the SSC dynamics in Indian Ocean. We also attempt to explain the significance of this impact.

A few studies have recently focused on the spatial variations in SSC dynamics associated with the 2004 Indian Ocean tsunami. Notable increases of SSC, along the Andhra and Tamilnadu coasts of India, were found after the tsunami (Anilkumar et al., 2006). A significant increase in SSC, around the estuaries of some large rivers, was also observed one month after the tsunami (Yan and Tang, 2008). These studies advanced our understanding of the influence of tsunamis on SSC in the coastal sea regions. However, questions still remain about various environmental factors which could have also affected the spatial and temporal dynamics of SSC around the tsunami, and how these environmental factors contributed to SSC variability and distribution.

* Corresponding authors. Fax: +86 02 89023203 (D.L. Tang), +86 931 8912481 (Z.Z. Li).
E-mail addresses: lingzistdl@126.com (D. Tang), zizhenlee@lzu.edu.cn (Z. Li).
URL: http://lingzis.51.net/ (D. Tang).

0025-326X/$ - see front matter © 2009 Elsevier Ltd. All rights reserved.
doi:10.1016/j.marpolbul.2009.04.023

Satellite remote sensing data have been widely used to study the spatial distributions of SSC, wind, sea surface temperature, phytoplankton, etc. at the sea surface (Bowers et al., 1998; Tang et al., 2004, 2006a,b; Zhao et al., 2008). Because of many contributing factors, such as tides, offshore distance, wind, rain, etc. the values of SSC among adjacent areas may not be independent but tend to be related, i.e., the SSC may be spatially clustered or spatially correlated. In this study, in order to solve the problem of spatial correlation in SSC, a spatial autoregressive model was used. We used satellite data to model the joint effects of rainfall (RF) and wind speed (WS) on SSC.

2. Study area and materials

The study area was located from 5°S to 11°N, 74°E to 98°E in the eastern Indian Ocean (Fig. 1), covering the epicenter, coastal seas and also some adjoining deep sea areas.

SSC is usually measured by satellites, from the observations of the normalized water-leaving radiance (NWR) values. The satellite SeaWiFS NWR value at 555 nm is related closely to the total SSC (Li et al., 2003; Mobasheri and Mousavi, 2004; Tan et al., 2006). NWR has thus been used as a substituted measure of SSC to study the spatial variability in SSC (Li et al., 2003; Mobasheri and Mousavi, 2004; Tan et al., 2007). Following these studies, we refer to NWR as SSC in this paper. Seven temporal periods (called "weeks" hereafter) were chosen, for the time period spanning 3 weeks before the tsunami week and 3 weeks after (Table 1).

The satellite SeaWiFS NWR 8-day data, 0.5° resolution at 555 nm (Level 3), were obtained from the Ocean Color Time Series Project (National Aeronautics and Space Administration, USA) (http://reason.gsfc.nasa.gov/Giovanni/). The satellite QuickScat wind data 0.25° resolution (Level 3) were obtained from the Jet Propulsion Laboratory (California Institute of Technology) (http://poet.jpl.nasa.gov/). The 0.25° resolution wind data were aggregated up to 0.5° resolution for the analysis together with other data at the same scale. Accumulated 8-day RF 0.5° resolution data, observed by satellite (Daily) TRMM (3B42 V6), were obtained via the TRMM Online Visualization and Analysis System (National Aeronautics and Space Administration, USA) (http://disc2.nascom.nasa.gov/Giovanni/tovas/). Level 3 data used in this study are high level data with research quality. To ensure the quality of the data, a very small portion of outliers and missing values were identified and excluded in the modeling.

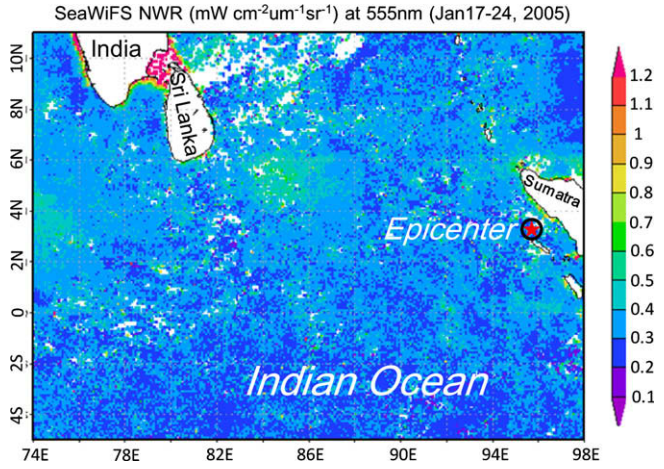

Fig. 1. SSC distribution in one week of January 17–24, 2005 in study area (5°S–11°N, 74°E–98°E). Epicenter is marked. The figure was generated by the Ocean Color Time Series Project (National Aeronautics and Space Administration, USA) (http://reason.gsfc.nasa.gov/Giovanni/).

3. Models and methods

3.1. Spatial models

The commonly used spatial autocorrelation indicator is Moran's I:

$$I = z'Wz/z'z, \quad z_i = y_i - \bar{y}, \quad i = 1, ..., n, \tag{1}$$

where y_i is the observation value of variable y (SSC) at the ith location. z' is the transpose of z. The row-standardized W is an n by n spatial weight matrix determined by the spatial configuration of the n locations as:

$$W_{ij} = C_{ij} \Big/ \sum_{j=1}^{j=n} C_{ij}, \quad i,j = 1, ..., n, \tag{2}$$

where $C_{ij} = 1$ if locations (or grids) i and j are immediate vertical and horizontal neighbors and 0 otherwise. Moran's I is an asymptotically normal distribution (Cliff and Ord, 1981). Its expectation is $-[1/(n-1)]$. It is to zero for large n. I value usually varies between -1 and $+1$. The closer the I value is to ± 1, the higher is the spatial positive (negative) autocorrelation.

Due to the existence of spatial autocorrelation in SSC, WS and RF, ordinary linear regression methods may give invalid or misleading results. In order to better and accurately model the joint effects of RF and WS on SSC, a widely used mixed autoregressive model with a spatially autocorrelated error term ε was introduced:

$$y = \beta_0 + X\beta + \varepsilon, \ \varepsilon = \lambda W\varepsilon + \mu, \tag{3}$$

where y is dependent variable (SSC), λ is the spatially dependent coefficient in spatial autoregressive structure for the error term ε. λ usually varies between -1 and $+1$. The closer the λ value is to 0, the lower is the autocorrelation in error term ε. W is n by n spatial weight matrix, associated with the spatial autoregressive process in the error term ε. β_0 is an intercept. β is a 2 by 1 vector of the parameters associated with explanatory variables $X = (WS, \log(RF + 1))$. The logarithm of RF was, from an exploratory data analysis, identified to have a linear relationship with SSC; thus, $\log(RF + 1)$ was used to avoid zeroes in the logarithm. The noise μ is normally distributed. Formula (3) is also called a spatial error model (SEM) since the spatial dependence is related to the error term.

For $\lambda = 0$, SEM model (3) is just the ordinary linear regression model (OLM):

$$y = \beta_0 + X\beta + \varepsilon, \tag{4}$$

3.2. Estimation and test methods

The significance of Moran's I values of SSC, RF, WS, OLM residuals and SEM residuals, measured by model (1), were tested using normal approximation. The test for the Pearson correlation coefficient r for WS, RF and SSC was conducted by the ordinary t-test. We then used formula (3) to model SSC (y) in relation to the explanatory variables $X = (WS, \log(RF + 1))$. The parameters of the SEM model (3) were estimated using the maximum likelihood method. Except for determining the significance of the spatial dependence coefficient λ by likelihood ratio test, the significance of all the other parameters was tested using the Wald test. The likelihood ratio statistic and Wald statistic are all asymptotically distributed as χ^2_q, where q is the number of degrees of freedom. The log-likelihood function and associated test methods are highly complicated, and will not be detailed here. For information about these specialized methods please refer to the work of Anselin (1988). The computations and test estimations were all implemented using the package of "spdep" of statistical software **R** (http://www.r-project.org).

Table 1
Moran's *I* tests for 5 items, and the Pearson correlation coefficient *r* test between WS, RF and SSC.

Index	Value\period (Week)	December 2–9 (a)	December 10–17 (b)	December 18–25 (c)	December 26–31 2004 (d)	January 1–8 2005 (e)	January 9–16 (f)	January 17–24 (g)
I	SSC	0.1616	0.2459	0.1586	0.2411	0.3045	0.3874	0.2263
	WS	0.8925	0.9041	0.8338	0.9035	0.8306	0.8581	0.9183
	RF	0.7895	0.7460	0.8424	0.7478	0.60	0.6441	0.5677
	OLM residuals	0.1156	0.2036	0.1584	0.1890	0.3022	0.2906	0.2052
	(All the above *P*-values < 0.00001)							
	SEM residuals	−0.0076	−0.0254	−0.0173	−0.0141	−0.0275	−0.0231	−0.0210
	P-Value	0.7881	0.3786	0.5862	0.6335	0.5624	0.4094	0.3284
r	SSC–WS	0.2204	0.2516	−0.0002	0.2523	−0.0004	0.1196	0.1642
	P-Value	9.8e−14	1.1e−15	0.9943	1.7e−15	0.9918	0.00014	1.04e−09
	SSC–RF	−0.0645	0.092	−0.0231	0.0592	−0.0794	−0.2677	0.1289
	P-Value	0.03123	0.00385	0.4938	0.06576	0.07211	2.2e−16	1.77e−06

4. Results

4.1. Spatial correlation analysis of SSC, WS and RF

There were significant spatial autocorrelations in the distributions of SSC, WS and RF for each week (Table 1), but the degree of this spatial correlation for WS and RF was obviously higher than that for SSC. The Pearson correlation *r* value test between WS, RF and SSC showed a significant positive correlation between SSC and WS (Table 1), but the significance of this positive relationship totally disappeared immediately before and after the tsunami week (Week d). The relationship between SSC and RF showed positive during some weeks and negative in other weeks. However, such positive or negative correlation displayed no statistical significance immediately around the tsunami week.

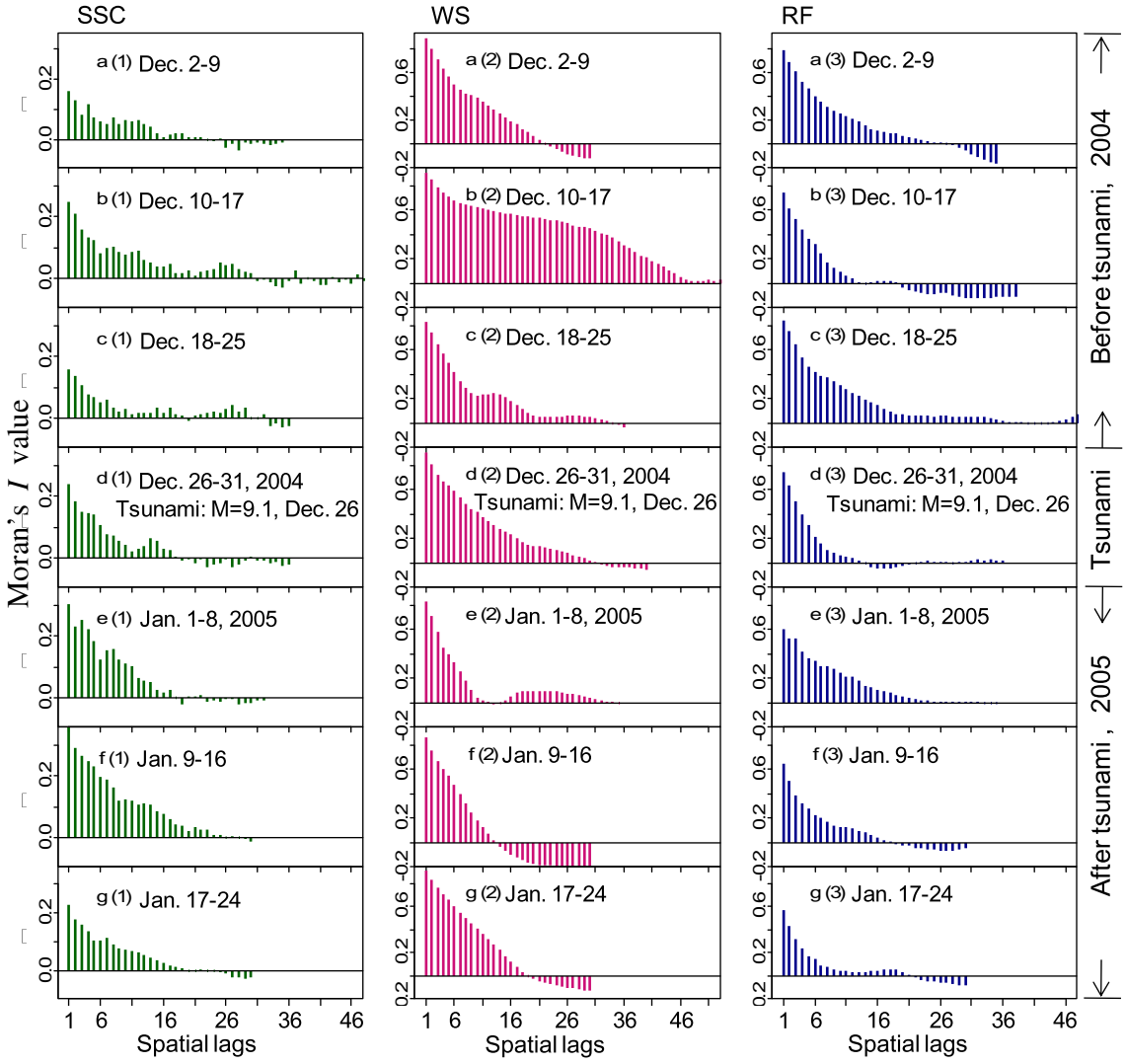

Fig. 2. Spatial correlograms for SSC, WS and RF. One spatial lag is in 0.5° unit. *X*-axis is the number of spatial lags. *Y*-axis is the Moran' *I* values. The first column is for SSC, the second column is for WS and the third column is for RF.

Comparison of the spatial correlograms of SSC, WS and RF (Fig. 2) showed a general trend of gradual decrease of the spatial autocorrelations in SSC, WS and RF along spatial lags. A noticeable fluctuation appeared in the correlograms of SSC, WS and RF around the tsunami event. The spatial correlograms in Week a and Week g are similar and decreased consistently, and thus may be considered as the "normal" correlograms.

4.2. Spatial and temporal series analysis among SSC, WS and RF

In order to capture the characteristics of the spatial distributions in SSC, WS and RF, we studied the series of the average of SSC, WS and RF extending outward from the epicenter, with a spatial interval (or lag) of 2° (called the "spatial series"). There were notable fluctuations in SSC, WS and RF for each week as spatial lags increased (Fig. 3), but the fluctuations in SSC, WS and RF all appeared markedly more intense around the tsunami week. This was especially the case for SSC (at spatial lag 1), WS (at spatial lag 6) and RF (at spatial lag 6) all of which increased considerably and reached their maximum values in Week e. The spatial series of SSC, WS and RF in Week a and Week g showed weaker fluctuations (Fig. 3a and g).

The temporal series of SSC, WS and RF showed that SSC and WS had a very similar increasing trend around the tsunami event (Fig. 4(1–3)). However, SSC and RF had no common or similar variation trend. The maximum values of SSC, WS and RF all appeared in Week e. In order to better understand the phenomenon as to why the maximum values of SSC, WS and RF all appeared in Week e (January 1–8, 2005), the temporal series of SSC, WS and RF in the week of January 1–8 from 2001 to 2005 were analyzed (Fig. 4(4–6)). There were no significant changes in SSC and WS in Week e compared with the same period (January 1–8) in the four earlier successive years (Fig. 4(4, 5)). Interestingly, the variation trends of SSC and WS were totally the same in the successive 5 years. The RF was remarkably higher in Week e and the average of RF (58.9 mm) in Week e exceeded twice the average of RF (26.6 mm) for the same period in the four earlier successive years.

4.3. The effects of WS and RF on SSC

Clearly, there was a significant autocorrelation in the residuals of the OLM model (Table 1). However the Moran's *I* values in the SEM residuals notably decreased compared with those in the OLM residuals, and they were all much smaller and close to zero

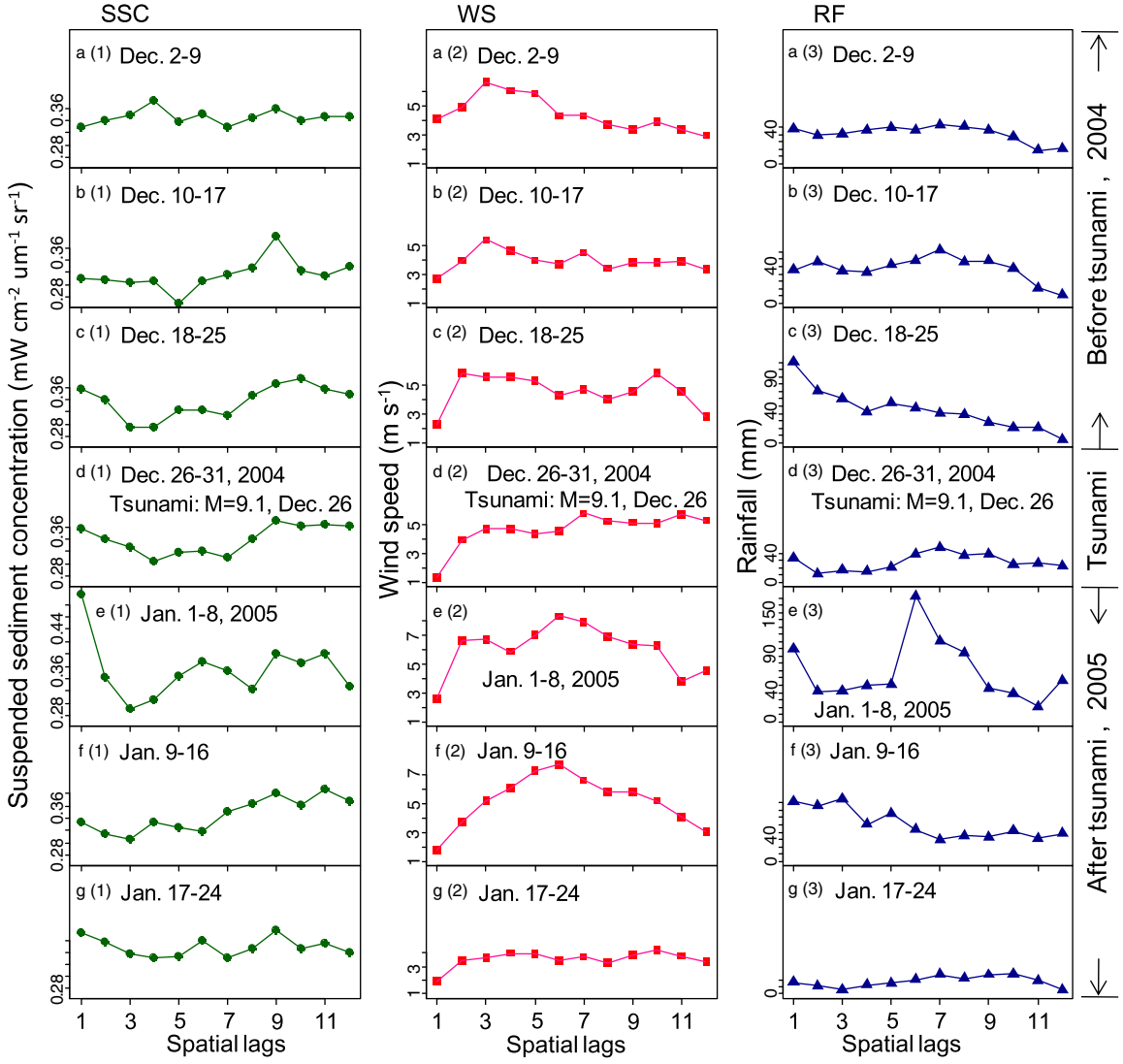

Fig. 3. Spatial series comparison among the average of SSC (mW cm^{-2} μm^{-1} sr^{-1}), RF (mm) and WS (m s^{-1}). One spatial lag is 2° away from the epicenter. *X*-axis is the number of spatial lags. *Y*-axis is the values of SSC, WS and RF, respectively. The first column is for SSC, the second column is for WS, and the third column is for RF.

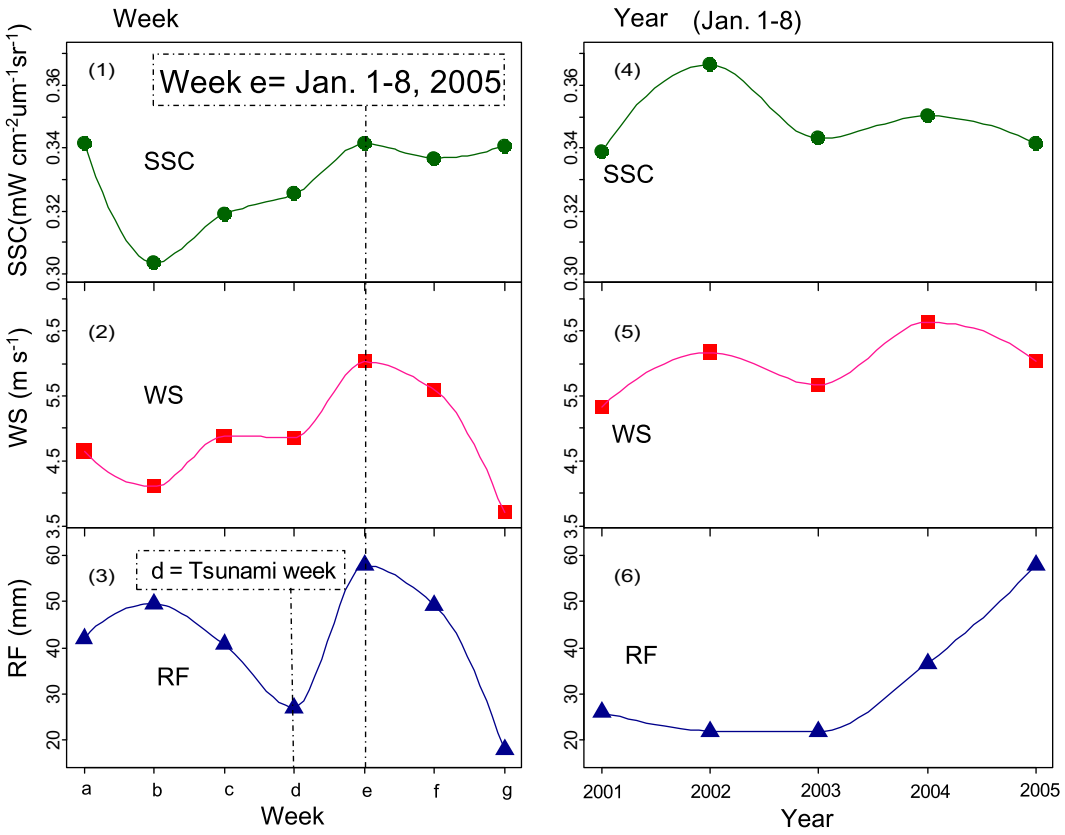

Fig. 4. Temporal series comparison among the averages of SSC (mW cm^{-2} μm^{-1} sr^{-1}), RF (mm) and WS (m s^{-1}). The first column is for the 7 weeks around the tsunami and the second column is for the week of January 1–8 in 5 years. a, b... g are the 7 weeks shown in Table 1.

with no test-significant autocorrelation for each week. Clearly the SEM model has effectively solved the problem of autocorrelation in OLM residuals. We then used the SEM model to model the joint effects of RF and WS on SSC.

The results showed that (Table 2): the high significance of λ values indicated that the SEM model fitted the data of RF, WS and SSC very well and it effectively captured the characteristics of the spatially autocorrelated distributions in SSC, WS and RF. WS had a positive effect on SSC except in Week c and Week e immediately before and after the tsunami week. The high *P*-values indicated that WS had no significant influence on SSC in Week c and Week e. Neither the positive nor the negative effects of RF on SSC were found to be consistent. RF had no significant influence on SSC around the tsunami event.

Table 2
Spatial autoregressive analysis for SEM model. a, b... g are the 7 weeks shown in Table 1.

Week\variable		β_0	WS	log(RF + 1)	λ
a	Coefficient	0.3263	0.00701	−0.00528	0.15996
	P-value	<2.2e−16	1.54e−10	0.01389	4.96e−06
b	Coefficient	0.27110	0.00697	0.00146	0.24297
	P-value	<2.2e−16	2.67e−11	0.5224	1.44e−12
c	Coefficient	0.31904	7.03e−05	1.65e−04	0.19929
	P-value	<2.2e−16	0.9667	0.9249	1.15e−07
d	Coefficient	0.28270	0.00725	0.00319	0.24422
Tsunami week	*P*-value	<2.2e−16	1.37e−10	0.1234	1.31e−11
e	Coefficient	0.35828	−0.00121	−0.00340	0.34454
	P-value	<2.2e−16	0.6086	0.1697	4.54e−14
f	Coefficient	0.35740	0.00364	−0.01387	0.38492
	P-value	<2.2e−16	0.00987	<2.2e−16	<2.2e−16
g	Coefficient	0.31680	0.00496	0.00299	0.30443
	P-value	<2.2e−16	2.61e−06	0.04302	<2.2e−16

5. Discussion

5.1. Characteristics of spatial correlation among SSC, WS and RF

Immediately around the tsunami week (Week d), the positive correlation between SSC and WS disappeared, and the correlation between SSC and RF, whether positive or negative, also disappeared or weakened. We also found noticeable fluctuations in the correlograms of SSC, WS and RF around the tsunami event (Fig. 2). Earthquakes and floods can greatly affect sediments and contaminants in the coastal zones, and can likewise induce sudden changes in the ocean–atmosphere interactions (Hayakawa et al., 1994; Krishnakutty, 2005). It thus appears that the tsunami-caused floods and earthquake-induced shaking during 2004 Indian Ocean event may have suddenly and significantly altered these fundamental ocean–atmosphere relationships, which in turn bring about disturbances in the spatial distributions of SSC, WS and RF and decrease the correlation between WS, RF and SSC.

5.2. Spatio-temporal series comparison among SSC, WS and RF

The fluctuations in SSC, WS and RF, along spatial lags, all appeared notably intense around the tsunami week (Fig. 3). In particular, SSC (at spatial lag 1), WS (at spatial lag 6) and RF (at spatial lag 6) increased and reached their maximum values immediately after the tsunami week (Fig. 3e(1)–e(3)). The maximum values of SSC, WS and RF also appeared in Week e (Fig. 4(1–3)). Rainfall-caused runoff and wind-induced circulation typically contribute to an order-of-magnitude increase in tidally averaged offshore flow, while waves and seiching motions from wind forcing usually cause an order-of-magnitude increase in tidally averaged SSC (Talke and Stacey, 2008). The mixed effects of tsunami-induced

huge tides, runoff, tsunami-affected circulation and air–sea interactions may have simultaneously driven up WS, RF and SSC immediately after the tsunami week.

The changes in SSC and WS were not significant in Week e compared with the same period of the four earlier successive years (Fig. 4(4, 5)). This tends to support the work of Singh et al. (2007), who reported that the changes for wind during the tsunami were not unique compared to earlier years. The RF was remarkably higher in Week e and the average of RF (58.9 mm) at this time exceeded twice the average of RF (26.6 mm) for the same period (January 1–8) in the four earlier successive years. The present results suggested that the tsunami may have significantly altered the atmosphere–ocean interaction processes and associated circulation, and increased the RF considerably following the tsunami event.

Interestingly, the variation trends of SSC and WS were very similar in the time series (Fig. 4(1 and 2), (4 and 5)). This closely positive relationship between SSC and WS was consistent with the significant positive correlation in the spatial distributions of SSC and WS (analyzed in Sections 4.1 and 5.1), and this is also verified in Section 5.3.

5.3. Effects of WS and RF on SSC

One of the preconditions of the ordinary linear regression method (OLM) is that the residuals of OLM must be independent. The significant autocorrelation in the residuals of the OLM model indicated that the results of the OLM model were invalid or misleading (Table 1). Such spatial autocorrelation, in the residuals of OLM model, may be partly caused by the mixed effects of significant spatial autocorrelations in SSC, WS and RF together with the physical perturbation from the tsunami. The very small and insignificant Moran's I values of SEM residuals indicated that the SEM model effectively solved the problem of autocorrelation in OLM residuals.

WS had positive effect on SSC except in Week c and Week e immediately around the tsunami week. The positive effects of WS on SSC in this study were also consistent with many works which reported that SSC are often positively affected by wind-induced wave resuspensions (Powell et al., 1989; Schoellhamer, 1996; Warner et al., 2004). However, the disappearance of the significant effect of WS on SSC, immediately around the tsunami week, may be directly affected by the tsunami event.

Neither the positive nor the negative effects of RF on SSC were consistent, but were nonetheless significant during the first week and the last two weeks (Table 2). However, RF had no significant influence, with neither positive nor negative effect, on SSC round the tsunami event. This was consistent with the results of the inconstant correlation between SSC and RF (Table 1, Fig. 4). The results of the spatial error model again indicated accurately that the weakening or disappearance of the effects of RF on SSC may be related to the tsunami event.

It is believed that SSC has a direct influence on pollutants in coastal seas (Eisma, 1981). SSC has been used as a surrogate for sediment-associated contaminants (SAC) in recent studies, and so physical processes that affect SSC also largely affect the concentrations of associated contaminants (Leatherbarrow et al., 2005; Schoellhamer et al., 2003, 2007). The mixed physical processes of tsunami-induced huge tides, runoff and tsunami-affected air–sea interactions may have directly affected the spatio-temporal variability of SAC, since it affected SSC, WS and RF significantly.

6. Conclusion

Significant spatial autocorrelations in the spatial distributions of SSC, WS and RF for each week around the 2004 Indian Ocean tsunami were observed in the present study. WS and SSC had a strong positive relationship, and WS had a positive effect on SSC during the tsunami. Both the positive and negative effects of RF on SSC were inconsistent; however, the positive effect of WS on SSC dramatically decreased or disappeared immediately around the tsunami week, with the comparable effect of RF on SSC disappearing or weakening considerably, immediately around the tsunami event. It is apparent that these changes might be related closely to the tsunami event, during which the tsunami-caused floods and earthquake-induced shaking might have suddenly and markedly disturbed the ocean–atmosphere interaction processes, and weakened the effects of WS and RF on SSC.

SSC, WS and RF increased remarkably and reached their maximum values immediately after the tsunami week. In particular, the average of RF (58.9 mm), immediately after the tsunami week, exceeded twice the average of RF (26.6 mm) for the same period in the four earlier successive years. Clearly, the mixed effects of tsunami-induced waves, runoff, and tsunami-affected air–sea interactions have significantly increased WS, RF and SSC immediately after the tsunami week. These mixed effects may have directly affected the spatio-temporal variations of SAC.

Acknowledgements

This work was supported by research grants awarded to Dr. Tang DL: 1, The National Natural Science Foundation of China (40576053 and 40811140533) and NSF of Guangdong (8351030101000002); 2, The Chinese Academy of Sciences (kzcx2-yw-226 and LYQ200701) and The CAS/SAFEA International Partnership Program for Creative Research Teams. Thanks to Dr. Michael Watson for his help in editing English, also to Dr. Charles Sheppard and reviewers for constructive suggestions.

References

Anilkumar, N., Sarma, Y.V.B., Babu, K.N., 2006. Post-tsunami oceanographic conditions in southern Arabian Sea and Bay of Bengal. Current Science 90 (3), 10.

Anselin, L., 1988. Spatial Econometrics: Methods and Models. Kluwer Academic, Boston. pp. 61–69.

Bowers, D.G., Boudjelas, S., Harker, G.E.L., 1998. The distribution of fine suspended sediments in the Irish Sea and its dependence on tidal stirring. International Journal of Remote Sensing 19, 2789–2805.

Cliff, A.D., Ord, J.K., 1981. Spatial Process: Models and Applications. Pion, London. pp. 46–51.

Dahdouh-Guebas, F., Koedam, N., 2006. Coastal vegetation and the Asian tsunami. Science 311, 37.

De Haas, H., Eisma, D., 1993. Suspended-sediment transport in the Dollard estuary. Netherlands Journal of Sea Research 31 (1), 37–42.

Eisma, D., 1981. Suspended matter as a carrier for pollutants in estuaries and the sea. In: Geyer, R.A. (Ed.), Marine Environmental Pollution, Dumping and Mining, vol. 2, Elsevier Oceanographic Series 27B, pp. 281–295.

Hayakawa, M., Fujinawa, Y., Evison, F.F., Shapiro, V.A., Varotsos, P., Fraser-smith, A.C., Molchanov, O.A., Pokhotelov, O.A., Enomoto, Y., Schloessin, H.H., 1994. What is the future direction of investigation on electromagnetic phenomena related to earthquake prediction. In: Hayakawa, M., Fujinawa, Y. (Eds.), Electromagnetic Phenomena Related to Earthquake Prediction. Terra Scientific Publishing Company (TERRAPUB), Tokyo, pp. 667–677.

Krishnakutty, N., 2005. Effects of 2004 tsunami on marine ecosystems – a perspective from the concept of disturbance. Current Science 90, 772–773.

Leatherbarrow, J.E., McKee, L.J., Ganju, N.K., Schoellhamer, D.H., Flegal, A.R., 2005. Concentrations and Loads of Organic Contaminants and Mercury Associated with Suspended Sediment Discharged to San Francisco Bay from the Sacramento-San Joaquin River Delta, California. RMP Technical Report. SFEI Contribution No. 405. San Francisco Estuary Institute, Oakland, CA.

Li, R.R., Kaufman, Y.J., Gao, B.C., Davis, C.O., 2003. Remote sensing of suspended sediments and shallow coastal waters. IEEE Transactions on Geoscience and Remote Sensing 41, 559–566.

Liu, P.L.F., Lynett, P., Fernando, H., Jaffe, B.E., Fritz, H., Higman, B., Morton, R., Goff, J., Synolakis, C., 2005. Observations by the international tsunami survey team in Sri Lanka. Science 308, 1595.

Mobasheri, M.R., Mousavi, H., 2004. Remote sensing of suspended sediments in surface waters, using Modis images. ISPRS 20th Congress, vol. 35, Istanbul, pp. 1682–1750.

Nittrouer, C.A., Kuehl, S.A., 1995. Geological significance of sediment transport and accumulation on the Amazon continental shelf. Marine Geology 125, 175–176.
Powell, T.M., Cloern, J.E., Huzzey, L.M., 1989. Spatial and temporal variability in South San Francisco Bay (USA). Horizontal distributions of salinity, suspended sediments, and phytoplankton biomass and productivity. Estuarine, Coastal and Shelf Science 28, 583–597.
Ramaswamy, V., Rao, P.S., Rao, K.H., Thwin, S., Rao, N.S., Raiker, V., 2004. Tidal influence on suspended sediment distribution and dispersal in the northern Andaman Sea and Gulf of Martaban. Marine Geology 208, 33–42.
Ridderinkhof, H., Van der Ham, R., Van der Lee, W., 2000. Temporal variations in concentration and transport of suspended sediments in a channel-flat system in the Ems–Dollard estuary. Continental Shelf Research 20, 1479–1493.
Schoellhamer, D.H., 1996. Factors affecting suspended-solids concentrations in South San Francisco Bay, California. Journal of Geophysical Research 101 (C5), 2087–12095.
Schoellhamer, D.H., 2002. Variability of suspended-sediment concentration at tidal to annual time scales in San Francisco Bay, USA. Continental Shelf Research 22, 1857–1866.
Schoellhamer, D.H., Shellenbarger, G.G., Ganju, N.K., Davis, J.A., McKee, L.J., 2003. Sediment dynamics drive contaminant dynamics. In: The Pulse of the Estuary: Monitoring and Managing Contamination in the San Francisco Estuary, San Francisco Estuary Institute, Oakland, CA, pp. 21–26. (<http://www.sfei.org/rmp/pulse/pulse2003.pdf>).
Schoellhamer, D.H., Mumley, T.E., Leatherbarrow, J.E., 2007. Suspended sediment and sediment-associated contaminants in San Francisco Bay. Environmental Research 105, 119–131.
Singh, R.P., Cervone, G., Kafatos, M., Prasad, A.K., Sahoo, A.K., Sun, D., Tang, D.L., Yang, R., 2007. Multi-sensor studies of Sumatra earthquake and tsunami of 26 December 2004. International Journal of Remote Sensing 28, 2885–2896.
Talke, S.A., Stacey, M.T., 2008. Suspended sediment fluxes at an intertidal flat: the shifting influence of wave, wind, tidal, and freshwater forcing. Continental Shelf Research 28, 710–725.
Tan, C.K., Ishizaka, J., Matsumura, S., Yusoff, F.M., Mohamed, M.I., 2006. Seasonal variability of SeaWiFS chlorophyll-a in the Malacca Straits in relation to Asian monsoon. Continental Shelf Research 26, 168–178.
Tan, C.K., Ishizaka, J., Manda, A., Siswanto, E., Tripathy, S.C., 2007. Assessing post-tsunami effects on ocean colour at eastern Indian Ocean using MODIS aqua satellite. International Journal of Remote Sensing 28, 3055–3069.
Tang, D.L., Kawamura, H., Dien, T.V., Lee, M.A., 2004. Offshore phytoplankton biomass increase and its oceanographic causes in the South China Sea. Marine Ecological Progress Series 268, 31–41.
Tang, D.L., Satyanarayana, B., Zhao, H., Singh, R.P., 2006a. A preliminary analysis of the Sumatran tsunami influence on Indian Ocean CHL-a and SST. Advances in Geosciences 5, 15–20.
Tang, D.L., Kawamura, H., Shi, P., Takahashi, W., Guan, L., Shimada, T., Sakaida, F., Isoguchi, O., 2006b. Seasonal phytoplankton blooms associated with monsoonal influences and coastal environments in the sea areas either side of the Indochina Peninsula. Journal of Geophysical Research 111, G01010.
Tang, D.L., Zhao, H., Satyanarayana, B., Zheng, G.M., Singh, R.P., Lv, J.H., 2009. Enhancement of chlorophyll-a in the northeastern Indian Ocean after the 2004 south Asian tsunami. International Journal of Remote Sensing, in press.
UNEP, 2005. After the Tsunami: Rapid Environmental Assessment. United Nations Environment Programme, Nairobi.
Witt, G., Siegel, H., 2000. The consequences of the Oder flood in 1997 on the distribution of polycyclic aromatic hydrocarbons (PAHs) in the Oder River estuary. Marine Pollution Bulletin 40 (12), 1124–1131.
Warner, J.C., Schoellhamer, D.H., Ruhl, C.A., Burau, J.R., 2004. Floodtide pulses after low tides in shallow subembayments adjacent to deep channels. Estuarine, Coastal and Shelf Science 60 (2), 213–228.
Yan, Z., Tang, D.L., 2008. Changes in suspended sediments associated with 2004 Indian Ocean tsunami. Advances in Space Research. doi:10.1016/j.asr.2008.03.002.
Zhao, H., Tang, D.L., Wang, Y., 2008. Comparison of phytoplankton blooms triggered by two typhoons with different intensities and translation speeds in the South China Sea. Marine Ecology Progress Series 365, 57–65.
Zheng, G., Tang, D.L., 2007. Offshore and nearshore chlorophyll increases induced by typhoon and typhoon rain. Marine Ecology Progress Series 333, 61–74.
Zonta, R., Collavini, F., Zaggia, L., Zuliani, A., 2005. The effect of floods on the transport of suspended sediments and contaminants: a case study from the estuary of the Dese River (Venice Lagoon, Italy). Environment International 31, 948–958.